DIRECT CONTROL OF TURBULENCE FOR IMPROVED PLASMA CONFINEMENT

T. Kinoshita
RIAM, Kyushu university
Kasuga, Japan
Email: t.kinoshita@triam.kyushu-u.ac.jp

Y. Morishita
Department of Nuclear Engineering, Kyoto University
Kyoto, Japan

N. Kenmochi
National Institute for Fusion Science
The Graduate University for Advanced Studies, SOKENDAI
Toki, Japan

T. Yokoyama
National Institutes for Quantum Science and Technology (QST)
Ibaraki, Japan

K. Tanaka
National Institute for Fusion Science
Toki, Japan
IGSES, Kyushu university
Kasuga, Japan

H. Funaba
National Institute for Fusion Science
Toki, Japan

Abstract

Turbulence-driven anomalous transport is one of the primary factors that degrade plasma confinement performance and remains a common challenge in both tokamaks and stellarators/heliotrons. In the Large Helical Device, as the plasma density is varied, a transition occurs between dominant turbulence regimes—ion temperature gradient turbulence and resistive interchange modes [1]. During this transition, both the turbulence amplitude and anomalous transport are minimized. Using an exhaustive search combined with a support vector machine, we investigated the conditions under which this turbulence transition occurs. As a result, it was demonstrated that the transition—namely, the condition under which turbulence is suppressed—can be reasonably approximated by the empirical relation $n_e = 4.20, T_e - 5.28$. In this study, by implementing real-time plasma control to actively maintain this condition, a sustained turbulence-suppressed state was achieved, leading to a significant improvement in confinement performance.

1. INTRODUCTION

Transport driven by turbulence is called anomalous transport and is the root cause of plasma confinement degradation. The ultimate goal of turbulence and transport studies in fusion research is to understand the characteristics of turbulence through measurements and simulations/theory, and to design reactors and plasma operations that suppress turbulence to achieve a high fusion triple product. The Large Helical Device (LHD) is among the largest stellarators/heliotrons located in Toki, Gifu, Japan. More than 30 world-class measurement systems, including two-dimensional phase contrast imaging (2D-PCI) for turbulence profile measurement [2] and Thomson scattering measurement for electron temperature and density profile measurement [3], are installed at LHD, making it a suitable device for turbulence study. Furthermore, LHD has an excellent superconducting coil system and a steady-state data acquisition system [4], which has realized 3-minute-period discharges, and more than 190,000 discharges have been performed so far, making it an attractive research target for machine learning and statistical analysis [5, 6]. Transport in LHD plasmas is not only neoclassical, but also anomalous transport due to turbulence plays an important role [7], and the underlying physics are extremely complex. From a recent study [1], it has been

reported that there are two confinement regimes, which are governed by different types of turbulence in the core region depending on the operating plasma parameters. Figure 1 shows the dependence of turbulence levels on electron density under the same magnetic configuration for three different heating conditions: one electron cyclotron resonance heating (ECRH) and two neutral beam injection (NBI) conditions. In each case, the heating parameters were kept fixed while the density was scanned. These figures plot the turbulence level (turbulence amplitude normalized by electron density) at normalized radius ρ=0.5-0.7 in the hydrogen plasma . Note, ρ is the radius normalized by the averaged minor radius, which includes 99 % electron kinetic energy [8]. The dominant turbulence mode switches from the ion temperature gradient (ITG) mode to the resistive interchange (RI) mode as the electron density increases. The transition occurs at approximately $n_e = 1.6 \times 10^{19}$, 2.0×10^{19}, and $3.4 \times 10^{19}, \mathrm{m}^{-3}$, respectively, which correspond to the densities at which turbulence is most strongly suppressed [1]. This turbulence mode switching condition is hereafter referred to as the turbulence transition condition (TTC). At the time of this transition, not only the turbulence level shown in Fig. 1 but also the anomalous transport is simultaneously minimized. Thus, the TTC represents an operational regime that is particularly important for achieving improved plasma confinement. Despite this potential, no successful real-time control strategies have yet been reported that directly target and suppress turbulence to enhance confinement performance. A key challenge in achieving such control lies in the fact that, as illustrated in Fig. 1, the conditions for turbulence suppression—including the TTC—vary with heating parameters even under identical magnetic configurations. This variability complicates the development of reliable control methods aimed at maintaining plasma conditions near the TTC. Furthermore, effective turbulence control requires high-precision, real-time diagnostics and readily accessible plasma control knobs—capabilities that are available in LHD, making it especially well-suited for such control studies. In this work, we employ machine learning techniques to identify the TTC for a specific magnetic configuration. Building on this, we implement real-time plasma control to maintain the plasma near the TTC and demonstrate the effectiveness of direct turbulence suppression in improving confinement performance.

The paper is organized as follows: Section 2 describes the method of identifying the TTC using a SVM. In Section 3, we present the TTC-based control experiment and compare turbulence and transport. Section 4 summarizes the findings and discusses their implications.

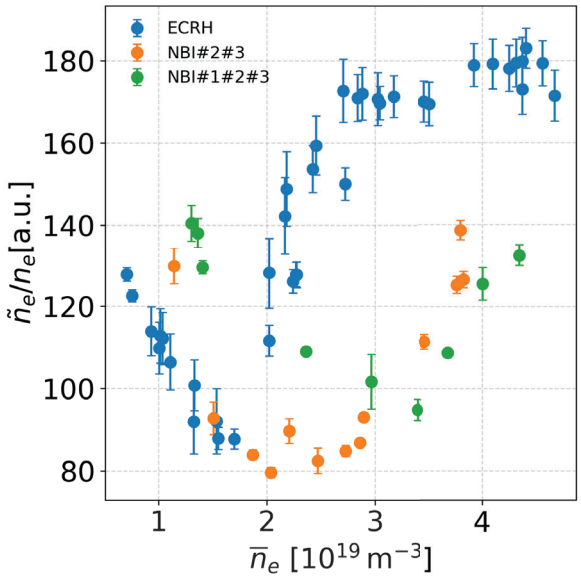

FIG. 1. Dependence of turbulence levels on electron density under different heating conditions in LHD

2. EXPLORING TURBULENCE TRANSITION CONDITION

2.1. Description of ES-SVM

As mentioned in Section 1, the TTC cannot be determined solely by electron density; rather, it must consider other parameters or a combination thereof. Since the TTC marks the boundary between two distinct turbulence regimes, classification algorithms specialized in boundary detection, such as Support Vector Machines (SVM), are well-suited for its identification. In this study, we focus on a magnetic configuration with a magnetic axis position $R_{ax} = 3.6\,\mathrm{m}$ and a toroidal magnetic field strength $B_t = 2.75\,\mathrm{T}$, which corresponds to the most typical

configuration in LHD where a sufficiently large dataset has been accumulated. The exploration of the TTC was conducted using 2000 datasets obtained under various heating conditions for the given magnetic configuration.

Figure 2 shows histograms of key plasma parameters averaged over the normalized radius $\rho = 0.5$–0.7, including electron density (n_e), electron temperature (T_e), ion temperature (T_i), the electron-to-ion temperature ratio (T_e/T_i), and their respective gradients: dn_e/dr, dT_e/dr, and dT_i/dr. These parameters play crucial roles in the stabilization or destabilization of ITG and RI. The red and blue histograms represent turbulence propagating in the ion-diamagnetic (i-dia.) and electron-diamagnetic (e-dia.) directions, respectively, as measured in the laboratory frame by 2D-PCI [2]. These propagation directions roughly correspond to ITG and RI turbulence, respectively. In this study, we employed a method combining exhaustive search (ES) over all parameter combinations and support vector machines, namely the Exhaustive Search with Support Vector Machine (ES-SVM) [9], to identify parameter sets capable of explaining the TTC. In fusion research, ES–SVM has been applied to estimate the likelihood of collapse (i.e., the probability of plasma disruption) in devices such as LHD and JT-60U [5, 10]. Prior to analysis, the input parameters for the ES-SVM were standardized. To enhance estimation accuracy and ensure the robustness of the model, we employed 10-fold cross-validation [11]. The classification performance was then assessed using the F1-score metric [12]. All procedures—including the Support Vector Machine, cross-validation, and F1-score calculation—were implemented using the Python `scikit-learn` library.

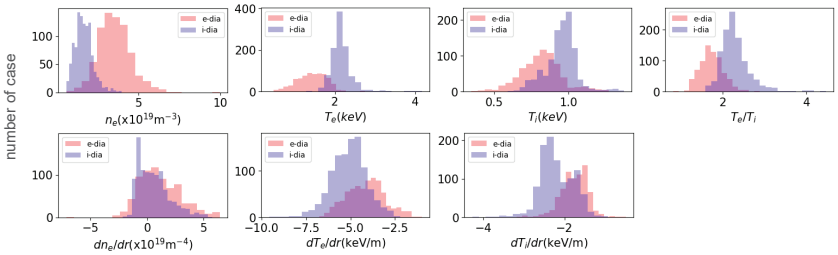

FIG. 2. Histograms of key plasma parameters in the dataset used for exploring the TTC

2.2. Classification result

Figure 3(a) shows, for each number of combined parameters (N), the parameter set that achieved the highest F1-score. For example, when $N = 1$, the best single parameter was T_e, which corresponds to the parameter highlighted in the histograms shown in Figure 2. For all combinations with $N > 1$, the F1-scores exceeded 0.9, indicating effective classification between ITG and RI regimes. The F1-score was maximized for the combination of three parameters ($N = 3$), specifically n_e, T_e, and dn_e/dr, with standardized coefficients of 3.07, -3.06, and -1.18, respectively. This classification result aligns well with the physical mechanism underlying the turbulence transition from ITG to RI as the density increases. The corresponding classification results are shown in panel (b), where the standardized parameters and their coefficients have been converted back to their original scales for easier interpretation. Misclassifications (marked by star symbols) mainly occur near the classification boundary (green line), where the turbulence amplitude tends to be low, indicating inherent uncertainty in this transitional region. However, in practical plasma operation, selectively controlling the electron density gradient is challenging. Fortunately, the combination of n_e and T_e alone achieves an F1-score exceeding 0.9. As shown in panel (c), the TTC can be effectively represented by the following boundary equation:

$$n_e = 4.20T_e - 5.28,$$

where n_e can be controlled by gas puffing and T_e by ECRH. Therefore, by maintaining the plasma conditions to consistently satisfy this relation, it is expected that turbulence will be continuously suppressed, thereby sustaining an improved confinement state.

3. REAL-TIME CONTROL EXPERIMENT

3.1. Experimental setup for control

The TTC is a function of both the electron density and electron temperature. In other words, for a fixed electron density, the TTC is uniquely determined by the electron temperature($T_{e,\mathrm{tgt}}$). In this approach, we aim to control the plasma to follow the TTC by adjusting the electron temperature using ECRH, while maintaining a constant electron density. That is, the plasma moves in the direction of the horizontal axis in Fig. 3(c) and converges at the cross-point to the TTC.

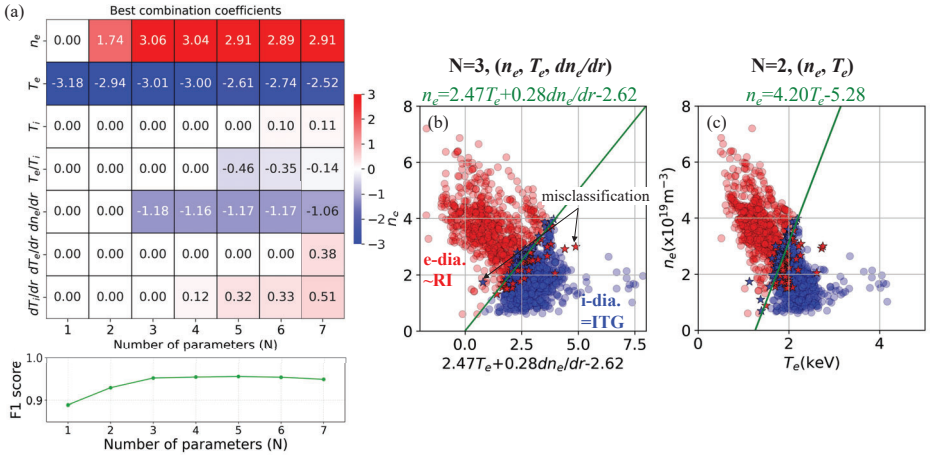

FIG. 3. (a)Best parameter combinations and their F1-scores, (b) ,(c)

The flowchart of temperature control approach is illustrated in Figure 4. After a plasma breakdown, the

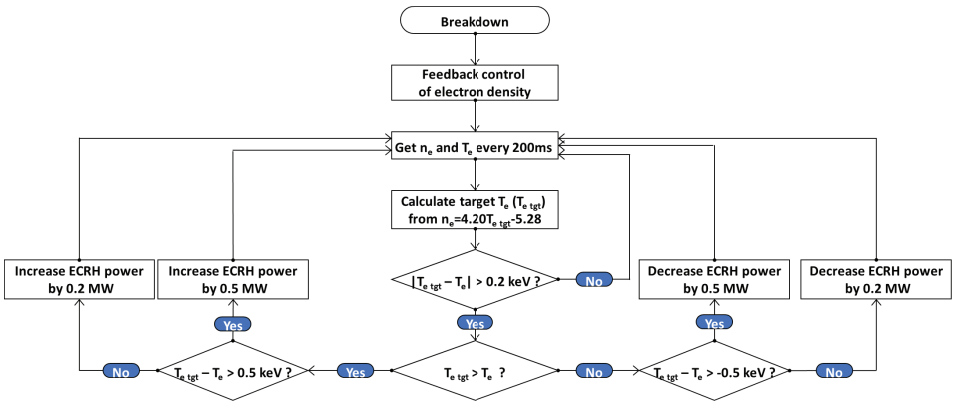

FIG. 4. Flowchart of temperature control approach

electron density is kept constant by a feedback control system based on line-integrated density measurements obtained from a far-infrared (FIR) laser interferometer [13]. This feedback control system is independent of the temperature control system. During this feedback control phase, the plasma is sustained by constant NBI heating, while ECRH is applied as needed to control the electron temperature. Whether or not to apply ECRH is determined by following process. To calculate $T_{e,\mathrm{tgt}}$ in real time, n_e and T_e measured by the Thomson scattering diagnostic [14] are used. The used values are averaged over the ranges of $R = 3.1$–3.3 m and $R = 4.0$–4.2 m, which approximately correspond to $\rho = 0.5$–0.7 in this magnetic configuration. Taking into account the signal transmission delay and the plasma response time to heating, data are acquired in real time every 200 ms. Then, by substituting n_e into the TTC equation ($n_e = 4.20T_e - 5.28$), the target electron temperature $T_{e,\mathrm{tgt}}$ that satisfies the TTC is calculated. The ECRH power is adjusted when the absolute difference between T_e and the target value $T_{e,\mathrm{tgt}}$ exceeds 0.2 keV. The individual ECRH powers are 337 kW (No. 1) and 380 kW (No. 2) at 77 GHz, and 389 kW (No. 4), 580 kW (No. 5), and 606 kW (No. 7) at 154 GHz. The total ECRH output from these five systems is adjustable in 32 discrete steps, with the maximum available power reaching 2290 kW. The change in heating power is either 200 kW or 500 kW, depending on the magnitude of the difference between T_e and $T_{e,\mathrm{tgt}}$.

3.2. Results of control experiment

Figure 5 shows the experimental results of temperature control. Panel (a) shows the time evolution of the electron density. Both the solid line and the symbols represent values measured by the Thomson scattering diagnostic; the solid line corresponds to post-processed data at 30 Hz, while the symbols indicate real-time processed data acquired every 200 ms, which are used in the control system. Red and blue indicate data with and without

temperature control, respectively. The electron density is maintained at approximately 1.0×10^{19} m^{-3} and 1.5×10^{19} m^{-3} during the highlighted orange and green periods, respectively (at $t = 3.2$–3.8 s and 4.4–5.0 s). Panel (b) shows the time evolution of the electron temperature. The lines, symbols, and their colors are consistent with those in panel (a). The dashed line represents the target temperature ($T_{e,\mathrm{tgt}}$), which is calculated from the electron density n_e using the TTC equation. Panel (c) displays the time evolution of the heating power. The dashed and solid lines represent the NBI heating power and ECRH power, respectively. For example, immediately after the change in electron density at $t = 4.0$ s, T_e is below $T_{e,\mathrm{tgt}}$ in both cases. In the controlled case, the heating power is subsequently increased, and approximately 400 ms later, at $t = 4.4$ s, T_e reaches $T_{e,\mathrm{tgt}}$. In contrast, without control, T_e remains clearly below the target temperature. As a result, as shown panel (d), the plasma is successfully controlled along the TTC line during the periods of $t = 3.2$–3.8 s and $t = 4.4$–5.0 s. In contrast, without control, the plasma deviates from the TTC line. To assess the effectiveness of this control, panel (e) presents the time evolution of the energy confinement time. The left-hand axis represents the normalized energy confinement time ($\tau_E/\tau_E^{\mathrm{ISS04}}$), while the right-hand axis represents the energy confinement time (τ_E). Where τ_E is the kinetic energy confinement time calculated by dividing the stored energy of electrons and ions by the deposited heating power, and τ_E^{ISS04} is the confinement time predicted by the international stellarator scaling law [15]. In the controlled case, the energy confinement time decreases because the heating power is increased to control the temperature. Therefore, to evaluate the effectiveness of the control while accounting for differences in heating power, we use the normalized energy confinement time, $\tau_E/\tau_E^{\mathrm{ISS04}}$. At an electron density of $n_e = 1.0 \times 10^{19}, \mathrm{m}^{-3}$, temperature control leads to a modest improvement in confinement, while at $n_e = 1.5 \times 10^{19}, \mathrm{m}^{-3}$, the improvement becomes considerably more pronounced.

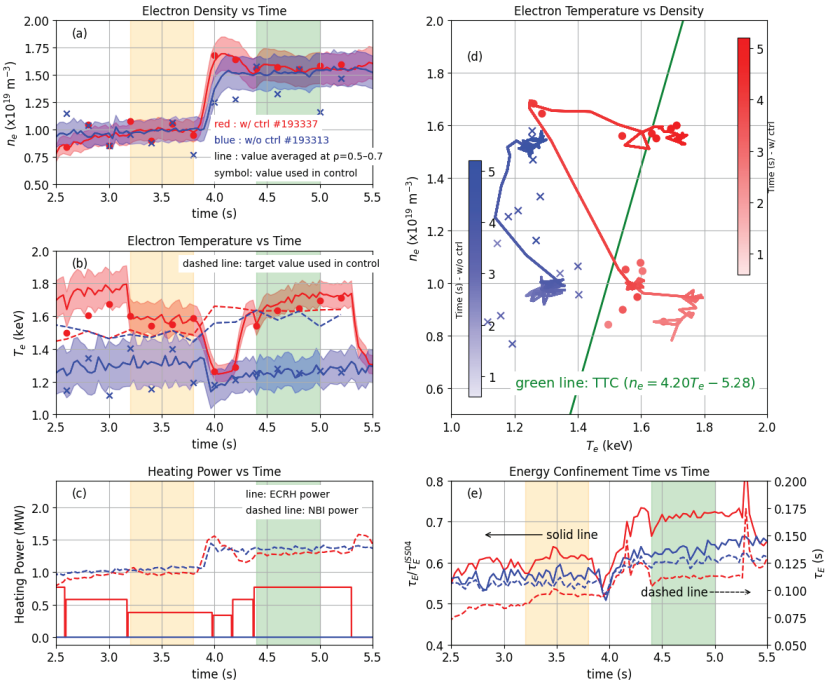

FIG. 5. Time evolutions of (a) electron density, (b) electron temperature, (c) heating power, and (e) energy confinement time, as well as (d) the relationship between electron temperature and electron density. The data are shown for the controlled discharge (#193337) and the uncontrolled discharge (#193313). The electron densities in both discharges are maintained constant at the highlighted periods.

Figure 6 compares the radial profiles of key plasma parameters at two time points. Panels (a), (b), and (c) correspond to $t = 3.5, \mathrm{s}$, when the electron density is maintained constant at $n_e = 1.0 \times 10^{19}, \mathrm{m}^{-3}$, while panels (d), (e), and (f) show the distributions at $t = 4.7, \mathrm{s}$, where n_e is maintained at $1.5 \times 10^{19}, \mathrm{m}^{-3}$. As shown in panels (a) and (c), the electron density profiles are identical at each respective timing. Panels (b) and (e) compare the electron and ion temperature profiles. In the temperature-controlled cases, the electron temperature is clearly elevated, which is attributed to ECRH applied for temperature control. In contrast, the ion temperature profiles remain nearly unchanged. This is likely due to the relatively low electron density, which results in insufficient energy transfer from electrons to ions through equipartition. Panels (c) and (f) show the radial profiles of density fluctuations measured by two-dimensional Phase Contrast Imaging (2D-PCI). In panel (c), which corresponds to the uncontrolled case, the turbulence exhibits a double-peaked structure with a prominent peak around $\rho = 0.8$

and a weaker peak near $\rho = 0.6$. When temperature control is applied, the turbulence near $\rho = 0.6$ is clearly suppressed, consistent with the fact that the TTC was explored based on the region $\rho = 0.5$–0.7. In contrast, in the case shown in panel (f), the turbulence around $\rho = 0.6$, which was previously weak as seen in panel (c), becomes significantly enhanced. Nevertheless, even under these enhanced turbulence conditions, applying temperature control successfully suppresses the turbulence.

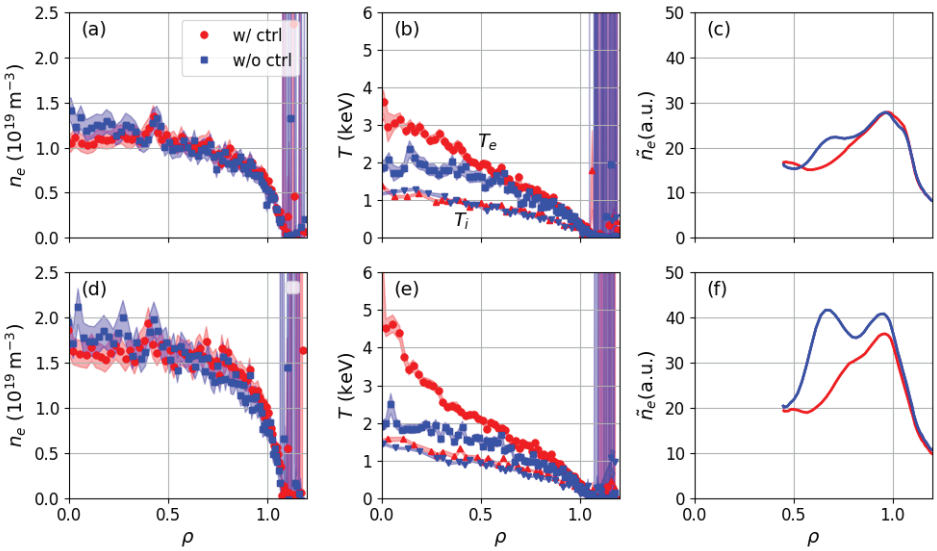

FIG. 6. Comparisons of Plasma Parameters and Turbulence at Two Density Conditions. Panels (a), (b), and (c) show the profiles at $n_e = 1.0 \times 10^{19}\,\mathrm{m}^{-3}$. Panels (d), (e), and (f) show the corresponding profiles at $n_e = 1.5 \times 10^{19}\,\mathrm{m}^{-3}$.

As described above, controlling the plasma temperature to follow the TTC resulted in a clear improvement in the normalized energy confinement time and significant suppression of turbulence. This indicates that the control successfully achieved its intended purpose of suppressing turbulence. However, the energy confinement time itself deteriorated. To investigate why the energy confinement time did not improve, a comparison of energy transport coefficients is presented in Fig .7. The solid line and dashed line indicate a experimental values and a neoclassical value, respectively. The experimental values were evaluated from a power-balance analysis using LHDGAUSS [16] and TASK3D [17], and the neoclassical values were calculated using DKES-PENTA [18]. As before, red represents the controlled case and blue represents represents the uncontrolled case. The electron and ion energy transport coefficients (χ_e and χ_i) at 1.0×10^{19} m^{-3} are shown in panels (a) and (b), respectively. As shown in panel (a), the experimental electron heat diffusivity (χ_e) is nearly identical for $\rho > 0.5$ between controlled and uncontrolled cases, while it is higher in the controlled case for $\rho < 0.5$, likely due to the additional ECRH heating. The neoclassical χ_e are comparable to or even exceed the experimental values, indicating a limited contribution from turbulence to electron heat transport. Panel (b) shows that the experimental ion heat diffusivity (χ_i) is slightly higher in the uncontrolled case for $\rho > 0.7$ and slightly higher in the controlled case for $\rho < 0.7$. In the uncontrolled case, the neoclassical χ_i is clearly lower than the experimental value, suggesting a significant contribution of anomalous transport and confinement degradation. In contrast, the controlled case shows close agreement between neoclassical and experimental χ_i, implying that neoclassical transport dominates under temperature control. Panels (c) and (d), corresponding to a higher electron density of 1.5×10^{19} m^{-3}, show similar trends to panels (a) and (b). Specifically, turbulence transport dominates in the uncontrolled cases, while neoclassical transport is predominant in the controlled cases. Overall, these results indicate that temperature control reduces turbulence-driven anomalous transport; however, this reduction is offset by an increase in neoclassical transport, leading to a slight deterioration in total heat transport. This is consistent with the observation that the energy confinement time slightly deteriorated under temperature control as shown in Fig. 5(e).

4. SUMMARY

In magnetically confined plasmas, turbulence plays a key role in determining plasma confinement. The suppression of turbulence during turbulence transition is a recently discovered phenomenon in LHD. While the turbulence transition observed between the ITG and RI regimes in LHD is a unique feature of its magnetic hill configuration,

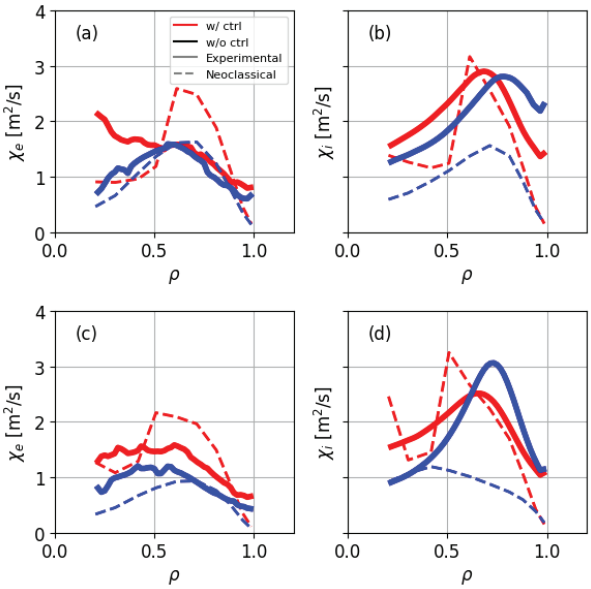

FIG. 7. Experimental and Neoclassical Heat Diffusivity of Electrons and Ions at Two Density Conditions. Panels (a) and (b) show the electron and ion heat diffusivity at $n_e = 1.0 \times 10^{19}\,\mathrm{m}^{-3}$. Panels (c) and (d) show the corresponding profiles at $n_e = 1.5 \times 10^{19}\,\mathrm{m}^{-3}$.

turbulence transitions themselves are common phenomena observed in both tokamaks and stellarators/heliotrons. This study was motivated by the observation that turbulence is reduced during ITG-RI transitions. This study aims to evaluate the effectiveness of real-time plasma control in improving confinement by satisfying the conditions under which turbulence suppression occurs. Prior to implementing control, we explored the TTC under various heating conditions for the given magnetic configuration using ES-SVM. As a result, we found that the combination of n_e and T_e, which are parameters externally controllable by gas puffing and ECRH, respectively, can approximately represent the TTC, expressed by the relation $n_e = 4.20T_e - 5.28$. Next, real-time control was implemented. In this study, T_e was controlled to satisfy TTC by adding ECRH to plasma with a constant density. This control resulted in the suppression of turbulence inside the plasma and the normalized energy confinement time was improved by up to 15%. However, this control method involves additional heating to satisfy the TTC, which decreases the energy confinement time by up to 5%. This was because total transport increased slightly due to temperature control. Without control, most of the transport was dominated by turbulent-driven anomalous transport, while with control, neoclassical transport dominated. The achievement of turbulence suppression and up to a 15% improvement in the normalized energy confinement time represents a clear success, demonstrating the effectiveness of the real-time control. However, the fact that this control method not only reduces turbulence but also increases transport through other mechanisms suggests that further optimization of the plasma control strategy is still required. In the current study, temperature control via ECRH did not consider its impact on transport in the inner region, specifically inside the normalized minor radius of ρ=0.5-0.7, which was the range used for TTC exploration. We are currently attempting density control using gas puffing, which is expected to be effective since it is less likely to affect the inner transport region as strongly as temperature control. Furthermore, in devices such as tokamaks, where neoclassical transport is already negligible compared to anomalous transport, this temperature control method is anticipated to be a powerful approach.

The data supporting the findings of this study are available in the LHD experiment data repository at `https://www-lhd.nifs.ac.jp/pub/Repository_en.html`. The authors would like to thank all the members of the LHD Experiment group for their excellent work. This work was supported by NIFS Grant (24KIPI001).

REFERENCES

[1] KINOSHITA, T. et al., Physical Review Letters **132** (2024) 235101.

[2] TANAKA, K. et al., Review of Scientific Instruments **79** (2008) 10E702.

[3] YAMADA, I. et al., Fusion Science and Technology **58** (2010) 345.

[4] NAKANISHI, H. et al., Fusion Engineering and Design **66** (2003) pp.

[5] YOKOYAMA, T. et al., Journal of Fusion Energy **39** (2020) 500.

[6] MORISHITA, Y. et al., Scientific Reports **14** (2024) 137.

[7] WARMER, F. et al., Physical Review Letters **127** (2021) 225001.

[8] SUZUKI, C. et al., Plasma Physics and Controlled Fusion **55** (2012) 014016.

[9] IGARASHI, Y. et al., Three levels of data-driven science, in *Journal of Physics: Conference Series*, volume 699, page 012001, IOP Publishing, 2016.

[10] YOKOYAMA, T. et al., Fusion Engineering and Design **140** (2019) 67.

[11] KOHAVI, R. et al., A study of cross-validation and bootstrap for accuracy estimation and model selection, in *Ijcai*, volume 14, pages 1137–1145, Montreal, Canada, 1995.

[12] DICE, L. R., Ecology **26** (1945) 297.

[13] AKIYAMA, T. et al., Fusion Science and Technology **58** (2010) 352.

[14] YAMADA, I. et al., Review of Scientific Instruments **87** (2016).

[15] YAMADA, H. et al., Nuclear Fusion **45** (2005) 1684.

[16] TSUJIMURA, T. I. et al., Nuclear Fusion **55** (2015) 123019.

[17] YOKOYAMA, M. et al., Nuclear Fusion **57** (2017) 126016.

[18] SPONG, D., Physics of plasmas **12** (2005).